ON THE INTERACTION BETWEEN FATIGUE CRACK BRANCHING AND CLOSURE

Marco Antonio Meggiolaro
Dept. of Mechanical Engineering - Pontifical Catholic University of Rio de Janeiro (PUC-Rio)
Rua Marquês de São Vicente, 225 Gávea, Rio de Janeiro, RJ 22453-900
meggi@mec.puc-rio.br

Antonio Carlos de Oliveira Miranda
Tecgraf - Pontifical Catholic University of Rio de Janeiro (PUC-Rio)
Rua Marquês de São Vicente, 225 Gávea, Rio de Janeiro, RJ 22453-900
amiranda@tecgraf.puc-rio.br

Jaime Tupiassú Pinho de Castro
Dept. of Mechanical Engineering - Pontifical Catholic University of Rio de Janeiro (PUC-Rio)
Rua Marquês de São Vicente, 225 Gávea, Rio de Janeiro, RJ 22453-900
 jtcastro@mec.puc-rio.br

Luiz Fernando Martha
Dept. of Civil Engineering - Pontifical Catholic University of Rio de Janeiro (PUC-Rio)
Rua Marquês de São Vicente, 225 Gávea, Rio de Janeiro, RJ 22453-900
lfm@tecgraf.puc-rio.br

Abstract. *The stress intensity factors (SIF) associated with branched fatigue cracks can be considerably smaller than that of a straight crack with the same projected length, causing crack growth retardation or even arrest. This mechanism can quantitatively explain retardation effects even when plasticity induced crack closure cannot be applied, e.g. in high R-ratio or in some plane strain controlled fatigue crack growth problems. Analytical solutions have been obtained for the SIF of branched cracks, however numerical methods such as Finite Elements (FE) or Boundary Elements (BE) are the only means to predict the subsequent curved propagation behavior. In this work, a FE program is developed to calculate the path and associated SIF of branched cracks, validated through experiments on 4340 steel ESE(T) specimens. From these results, semi-empirical crack retardation equations are proposed to model the retardation factor along the crack path. The model also considers the possible interaction between crack branching and other retardation mechanisms.*

Keywords*: Crack retardation model, Bifurcated cracks, Finite elements, Life prediction.*

1. Introduction

Fatigue cracks can significantly deviate from their Mode I growth direction due to the influence of overloads, multi-axial stresses, micro structural inhomogeneities such as grain boundaries and interfaces, or environmental effects, generating crack kinking or branching (Lankford and Davidson, 1981). A fatigue crack deviated from its nominal Mode I plane induces mixed-mode near-tip conditions even if the far-field stress is pure traction. For instance, a pure Mode I stress intensity factor (SIF) K_I induces Modes I and II SIF k_1 and k_2 near the longer branch of a bifurcated crack and k_1' and k_2' near the shorter one. The equivalent SIF K_b and K_c of the longer and shorter branches, calculated respectively from (k_1, k_2) and (k_1', k_2') using e.g. the $\sigma_{\theta max}$ criterion (Erdogan and Sih, 1963), can be considerably smaller than that of a straight crack with the same projected length. Therefore, such branching can retard or even arrest subsequent crack growth (Suresh, 1983).

It is experimentally observed that very small differences between the crack branch lengths b and c are enough to cause the shorter branch c to arrest while the longer one b propagates, generally changing its curvature at a retarded rate until returning approximately to its pre-overload SIF and growth direction and rate. Therefore, although many branches can be developed along the main crack path, only the fastest branch continues to grow, while all others are brought to a stop due to a shielding effect. This typical propagation behavior has been observed in many structural components.

Some analytical solutions have been obtained for the SIF of kinked and branched cracks, but it is generally recognized that it is very difficult to develop accurate analytical solutions to their complex propagation behavior (Karihaloo, 1982). Therefore, numerical methods such as Finite Elements (FE) and Boundary Elements (BE) are the only practical means to predict the propagation behavior of branched cracks (Pärletun, 1979). A summary of such SIF solutions as a function of the deflection angle and the length of the deflected part of the crack is presented in (Suresh and Shih, 1986).

To predict the (generally curved) path of a branched crack and to calculate the associated Modes I and II SIF, a specially developed interactive FE program named Quebra (meaning fracture in Portuguese) is used (Miranda et al.,

2002). This program simulates two-dimensional fracture processes based on a FE self-adaptive strategy, using appropriate crack tip elements and crack increment criteria.

2. Propagation of branched cracks

The growth of branched cracks is studied using the Quebra program to model a C(T) specimen with width $w = 32.0mm$, crack length $a = 14.9mm$, and a very small bifurcation with angle 2θ ranging from 40° to 168°, initial longer branch length $b_0 = 10\mu m$ and initial shorter branch lengths ranging from $c_0 = 5\mu m$ to $10\mu m$. A fixed crack growth step of $\Delta b = 3\mu m$ (or $1\mu m$ during the first propagation steps) is considered for the propagation of the longer branch b. This growth step is calculated in the direction defined by the $\sigma_{\theta max}$ criterion (Erdogan and Sih, 1963). Due to the differences in the SIF and crack growth rate, a growth step Δc smaller than Δb is expected for the shorter branch. This smaller step is obtained assuming a crack propagation law that models the first two growth phases:

$$\frac{da}{dN} = A \times (\Delta K - \Delta K_{th})^m \qquad (1)$$

where A and m are material constants and ΔK_{th} is the propagation threshold at a given R ratio. If ΔK_b and ΔK_c are respectively the stress intensity ranges of the longer and shorter branches, then the growth step Δc of the shorter branch c should be

$$\Delta c = \Delta b \cdot (\frac{\Delta K_c - \Delta K_{th}}{\Delta K_b - \Delta K_{th}})^m \qquad (2)$$

Interestingly, the ratio between the propagation rates of the two branches is independent of the material constant A. In this analysis, the exponent m is assumed to be 2.0, 3.0, or 4.0, which are representative for the range of the measured exponents for structural alloys. A similar expression can be obtained if other crack retardation mechanisms are considered, through Lang and Marci's (1999) propagation threshold K_{PR} with A and m parameters fitted for each considered load ratio R:

$$\Delta c = \Delta b \cdot (\frac{K_{\max,c} - K_{PR}}{K_{\max,b} - K_{PR}})^m \qquad (3)$$

where $K_{max,b}$ and $K_{max,c}$ are the maximum SIF of the longer and shorter branches respectively. This threshold K_{PR} can be interpreted as the limiting value K_{max}^* of the Unified Approach (Sadananda et al., 2001).

Both the crack path and the associated SIF along each branch are obtained using the Quebra program. Several calculations are performed for different values of the exponent m, bifurcation angle 2θ, relation c_0/b_0, and SIF, considering or not the effect of K_{PR}, as described next.

2.1. Branched crack propagation with $K_{PR} = 0$

In this section, the propagation behavior of branched cracks is studied using FE but neglecting any retardation mechanism other than the bifurcation itself (i.e. assuming $K_{PR} = 0$). Figure 1(a) shows the crack paths obtained from the FE analyses of bifurcated cracks with $2\theta = 130^o$ and $c_0/b_0 = \{0.5, 0.8, 0.95, 1\}$, considering $m = 2$ and $K_{PR} = 0$. The dashed lines show the theoretical propagation behavior of a perfectly symmetric bifurcation ($c_0/b_0 = 1$). In this case, the retardation effect would never end because both branches would propagate symmetrically without arresting. Clearly, such behavior is not observed in practice, since the slightest difference between b_0 and c_0 would be sufficient to induce an asymmetrical behavior. Figure 1(a) also shows that lower c_0/b_0 ratios result in premature arrest of the shorter crack branch, leading to smaller retardation zones. Also, the propagation path of the longer branch is usually restrained to the region within the dashed lines, while the shorter one is "pushed" outside that envelope due to shielding effects.

The size of the retardation zone can be estimated from the ratio b_f/b_0, where b_f is the value of the length parameter b of the longer branch (measured along the crack path) beyond which the retardation effect ends. The ratio b_f/b_0 is then calculated through FE propagation simulations for all combinations of $c_0/b_0 = \{0.5, 0.8, 0.9, 0.95\}$, $2\theta = \{40^o, 80^o, 130^o, 168^o\}$ and $m = \{2, 3, 4\}$, and fitted by the proposed empirical function:

$$\frac{b_f}{b_0} = \exp\left(\frac{2\theta - 30^o}{56 + 17 \cdot (m-2)^{2/3}}\right) \Big/ (1 - c_0/b_0)^{(12-m)/20}$$

$$(4)$$

Figure 1(b) shows a comparison between the fitted and the FE-obtained data for $m = 3$. Note that a greater symmetry between the branches (as c_0/b_0 approaches 1.0) results in a longer retardation zone, as expected from the delayed arrest of the shorter branch.

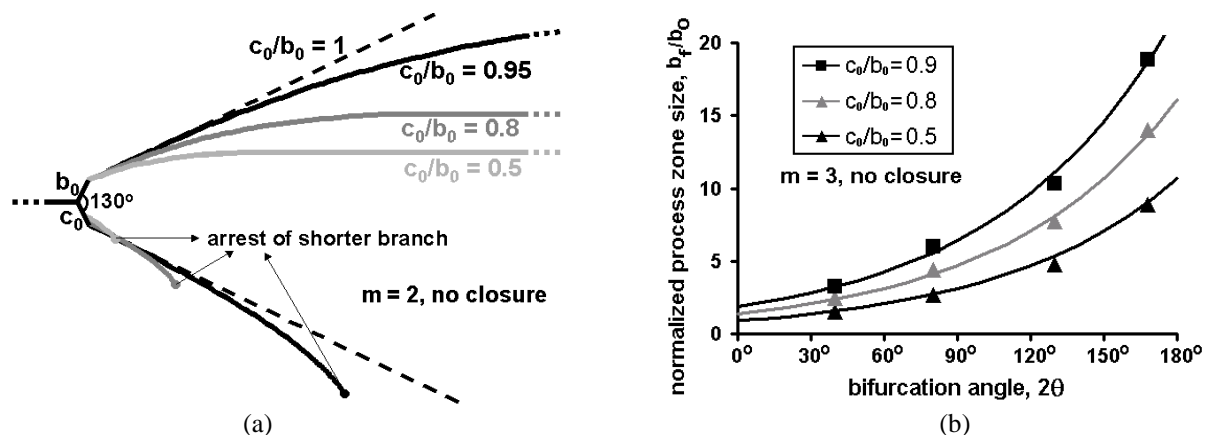(a)   (b)

Figure 1. (a) Bifurcated crack paths for several c_0/b_0 ratios ($m = 2$, $K_{PR} = 0$). (b) Normalized process zone size as a function of the bifurcation angle and branch asymmetry c_0/b_0 ($m = 3$, $K_{PR} = 0$).

The FE-calculated equivalent SIF K_b and K_c of the longer and shorter branches are now evaluated along the obtained crack paths. Figure 2 plots the crack retardation factors (defined as the ratios between K_b or K_c and the Mode I SIF K_I of a straight crack) for $2\theta = 130^o$ and $m = 2$, as a function of the normalized length $(b-b_0)/b_0$ of the longer branch. Because of the different crack branch lengths, the SIF at the longer one is much higher than that at the shorter branch. Assuming K_b and K_c to be the crack driving force, it can be seen from Fig. 2 that the longer branch reaches its minimum propagation rate right after the bifurcation occurs, returning to its pre-overload rate as the crack tip advances away from the influence of the shorter branch. As seen in the figure, the retardation behavior is misleadingly similar to closure-related effects, even though no closure is present in that case.
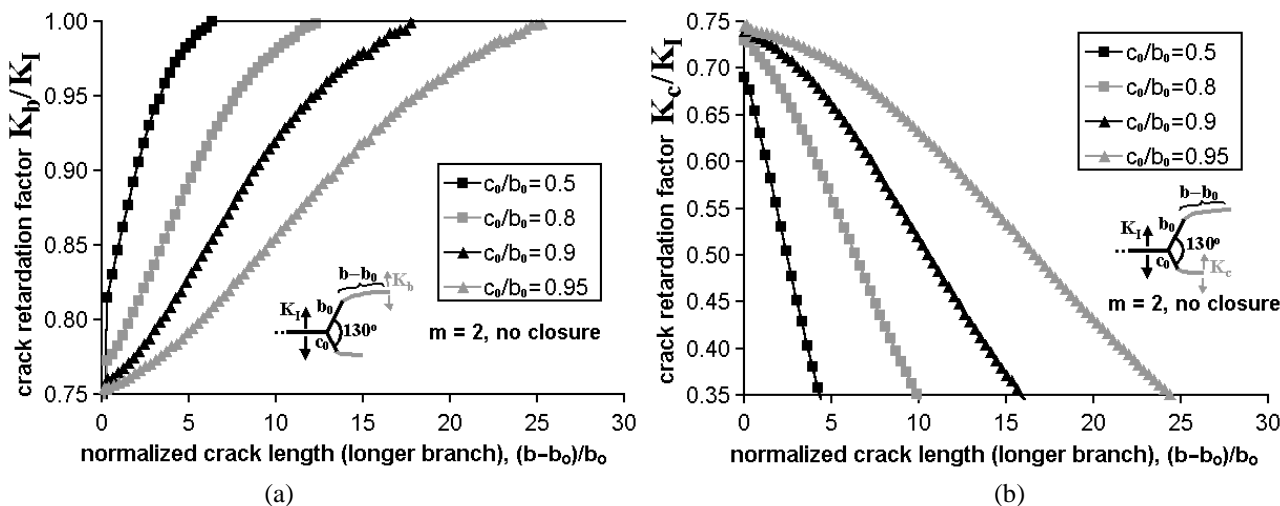

(a)   (b)

Figure 2. Normalized equivalent SIF for the (a) longer and (b) shorter branch of a bifurcated crack during its propagation ($2\theta = 130^o$, $m = 2$, $K_{PR} = 0$).

In addition, as the length difference between both branches increases, it is expected that the propagation rate of the shorter one is reduced until it arrests, after which the larger branch will dominate. Note that even small differences between the branch lengths, such as in the case $c_0/b_0 = 0.95$ shown in Fig. 2, are sufficient to cause subsequent arrest of the shorter branch.

An empirical expression is here proposed to model the SIF K_b of the longer branch during the transition between K_{b0} (the value of K_b immediately after the bifurcation event) and the straight-crack K_I (after the retardation effect ends), valid for $b_0 \le b \le b_f$ and $0.7 < c_0/b_0 < 1$:

$$K_b = K_{b0} + (K_I - K_{b0}) \cdot \left[a\tan\left(3\frac{b-b_0}{b_f-b_0} \right) / 1.25 \right]^{2c_0/b_0} \tag{5}$$

where b_f is given in Equation (4) and K_{b0} (and K_{c0}) by

$$\frac{K_{b0}}{K_I} = 0.75 + (1 - \sin\theta)\cdot\left(1 - \frac{c_0}{b_0}\right), \quad \frac{K_{c0}}{K_I} = 0.75 - (1 - \sin\theta)\cdot\left(1 - \frac{c_0}{b_0}\right) \tag{6}$$

It must be pointed out, however, that the presented FE results and empirical models might have some limitations, because actual bifurcations can be of a size comparable to the scale of the local plasticity (e.g., of the plastic zone size) or microstructural features (e.g., of the grain size). Moreover, possible environmental effects should be considered when comparing the bifurcation model predictions with measured crack growth rates (Suresh, 1983). The interaction between crack branching and other retardation mechanisms is studied next.

2.2. Influence of other mechanisms on branched crack propagation

All presented branched growth simulations so far have not included the effect of other retardation mechanisms. This effect is easily accounted for in the FE calculations using Equation (3). The limiting value K_{PR} is assumed to be the same at both branch tips and always larger than the minimum SIF of each branch. Further simulations are then conducted considering several K_{PR} values, normalized by the maximum Mode I SIF K_I of the straight crack, namely $K_{PR}/K_I = \{0.067, 0.08, 0.10, 0.13, 0.20, 0.25, 0.40, 0.57\}$.

A generalized version of Equation (4) is then proposed to fit the calculated process zone sizes including the combined effects of other mechanisms:

$$\frac{b_f}{b_0} = \frac{\alpha}{(1 - c_0/b_0)^{(12-m)/20}}\cdot\exp\left[\frac{-\beta}{(1 - c_0/b_0)^{\gamma}}\cdot\frac{K_{PR}}{K_I}\right] \tag{7}$$

where

$$\alpha = \exp\left(\frac{2\theta - 30^o}{56 + 17\cdot(m-2)^{2/3}}\right) \tag{8}$$

$$\beta = \left(\frac{2\theta}{110 + 60\cdot(m-2)^{0.6}}\right)^{5/2} \tag{9}$$

$$\gamma = \frac{180^o - 2\theta}{280 - 130\cdot(m-2)^{0.3}} \tag{10}$$

Note that the ratio K_{PR}/K_I in Equation (7) should be replaced with zero if K_{PR} is smaller than the minimum SIF of both branches. Figure 3 shows the comparison between the fitted and the FE-obtained data as a function of the ratio K_{PR}/K_I. Note that greater K_{PR} levels result in shorter retardation zones, because the shorter branch is more easily arrested due to the reduction in its stress intensity range.
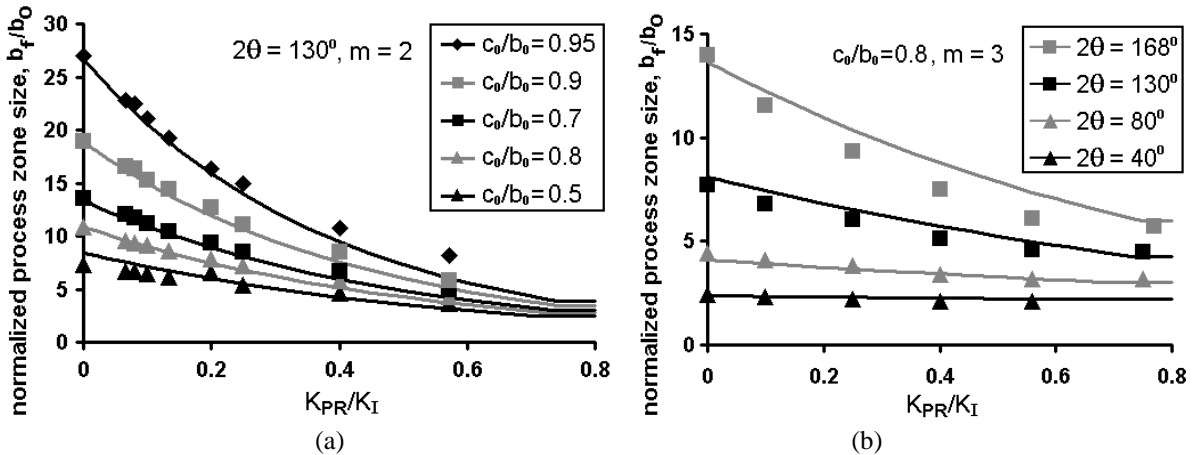

Figure 3. Normalized process zone size of bifurcated cracks as a function of K_{PR} for several (a) branch asymmetry ratios c_0/b_0 ($2\theta = 130^o$, $m = 2$); (b) bifurcation angles 2θ ($c_0/b_0 = 0.8$, $m = 3$).

Figure 4 shows the effect of K_{PR} at the branch tips on the retardation factor for $2\theta = 130^o$, $c_0/b_0 = 0.9$ and $m = 2$. Note that higher K_{PR} levels reduce the size of the retardation process zone, due to premature arrest of the shorter branch. In Fig. 4, e.g., the normalized size of the process zone is reduced from *18* to *3.6* as K_{PR}/K_I approaches *0.74*, a factor of *5*. In this example, *0.74* is the minimum K_{PR}/K_I level that prevents the shorter branch to even start propagating. Therefore, at any level above *0.74* the normalized process zone size will also be *3.6*, because the propagation geometry will remain unchanged as long as the shorter branch remains arrested at $c = c_0$.

Note, however, that a smaller process zone does not necessarily mean fewer delay cycles, since the longer branch will also experience a reduction in the crack propagation rate due to other retardation mechanisms. Therefore, a competition between lower growth rates of the longer branch and smaller bifurcation process zone sizes will take place to determine the real effect of combining bifurcation with other retardation mechanisms.

Equations (7-10) and (6) can then be applied to Equation (5) to model the SIF K_b of the longer branch during the transition between K_{b0} (the SIF immediately after the bifurcation event) and the straight-crack K_I (the SIF after the end of the retardation effect), completing this analysis.
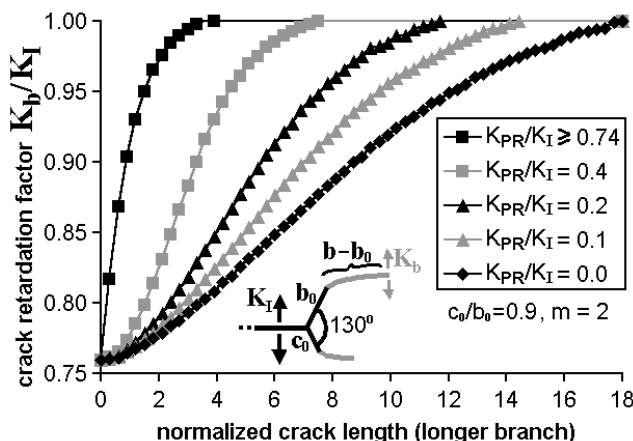

Figure 4. Normalized SIF of the longer branch during its propagation as a function of the normalized length $(b-b_0)/b_0$ for several K_{PR} levels ($c_0/b_0 = 0.9$, $m = 2$).

3. Experimental results

Quantitative validations of the predicted bifurcated crack growth behavior are performed on Eccentrically-loaded Single Edge Crack Tension specimens ESE(T) made from an annealed SAE 4340 alloy steel with $S_Y = 377$MPa, $S_U = 660$MPa, $E = 205$GPa, and $RA = 52.7\%$, and with the analyzed weight percent composition: C 0.37, Mn 0.56, Si 0.14, Ni 1.53, Cr 0.64, Mo 0.18, S 0.04, P 0.035. The tests are performed at frequencies between 20 and 30Hz in a 250kN computer-controlled servo-hydraulic testing machine. The crack length is measured following ASTM E 647 procedures (ASTM E647). Special attention is given for crack closure measurement. For this, a system with a high speed data acquisition is used to obtain data and to avoid intervention during the tests. In this way, the load and Crack-Opening Displacement (COD) data are used to compute the crack closure load using a digital linearity subtractor output, a circuit developed to precisely measure the opening load (Castro, 1993).

The proposed retardation equations are implemented in a fatigue life assessment program named ViDa (Miranda et al., 2002; Miranda et al., 2003). This program is used to estimate the number of delay cycles associated with the experimentally obtained bifurcation on the 4340 steel ESE(T) specimens. The number of cycles spent during the propagation in the retardation region is then calculated by integrating the *da/dN* equation along the longer crack branch, from $b = b_0$ to $b = b_f$.

Two tests are performed on ESE(T) specimens subject to 100% overloads, namely tests I and II: (I) $R = 0.7$, $\Delta K = 13.9$MPa√m, resulting in approximately 22,000 delay cycles; (II) $R = 0.05$, $\Delta K = 16.2$MPa√m, resulting in approximately 32,000 delay cycles, see Figs. 5-7.

It is found that the minimum load levels in test I is always above the opening load, therefore no crack closure is present neither before nor after the overloads. The measured initial branch lengths are approximately $b_0 = 9\mu m$ and $c_0 = 8.5\mu m$, with a bifurcation angle $2\theta = 160^o$, see Fig. 5(a). The material is modeled using Equation (1) with crack growth constants $A = 9 \cdot 10^{-11}$ m/cycle and $m = 2.1$, and a propagation threshold $\Delta K_{th} = 2.8$MPa√m, measured under $R = 0.7$. From Equation (6), it is found that $K_{b0}/K_I = 0.751$ and $K_{c0}/K_I = 0.749$, leading to $\Delta K_{b0} = 0.751 \cdot \Delta K_I = 10.437$MPa√m and $\Delta K_{c0} = 0.749 \cdot \Delta K_I = 10.413$MPa√m. Since both ranges are greater than $\Delta K_{th}(R=0.7) = 2.8$MPa√m, both branches are expected to start propagating, as verified experimentally. The size of the process zone can be estimated from Equation (4), which results in $b_f = 36.95 \times 9\mu m \cong 332\mu m$. The number of delay cycles n_D is then calculated by:

$$n_D = \int_{b_0}^{b_f} \frac{db}{A(\Delta K_b - \Delta K_{th})^m} - \int_{b_0}^{b_f} \frac{db}{A(\Delta K_I - \Delta K_{th})^m} =$$

$$= \int_9^{332} \frac{db \times 10^{-6}}{9 \cdot 10^{-11} \left\{ 7.64 + 2.27 \cdot \left[atan\left(3\frac{b-9}{332-9}\right)/1.25 \right]^{1.88} \right\}^{2.1}} - \int_9^{332} \frac{db \times 10^{-6}}{9 \cdot 10^{-11}(13.9-3.8)^{2.1}} = 9,664 \; cycles \tag{11}$$

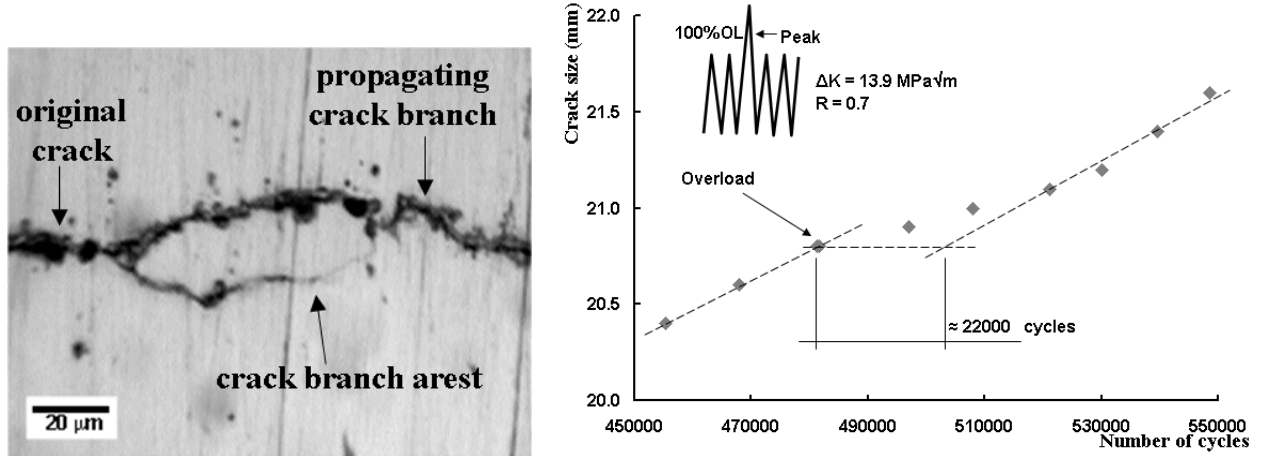which is approximately half of the measured 22,000 delay cycles, see Figure 5(b).

Figure 5. (a) Crack bifurcation experiments on SAE 4340 steel, test I. (b) Fatigue crack growth retardation after a 100% overload, $R = 0.7$ (test I).

Careful inspection of the fracture surfaces using a scanning electron microscope revealed a bifurcation front along the specimen thickness, see Fig. 6. Despite its 3-D geometry, the retardation behavior is still reasonably reproduced by the proposed 2-D model within a factor of 2 in number of delay cycles.
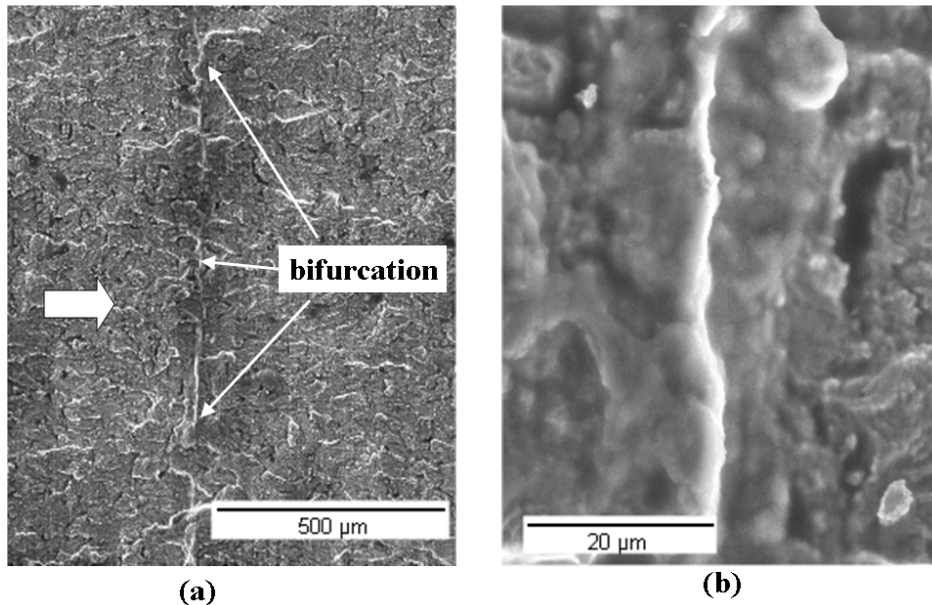

Figure 6. Scanning electron micrographs of fracture surfaces (test I): (a) bifurcation front through the specimen thickness, and (b) detailed view indicating different height levels.

For test II, the initial branch lengths are approximately $b_0 = 10\mu m$ and $c_0 = 9.5\mu m$, with a bifurcation angle $2\theta = 150^o$. The material is modeled using Equation (1) with crack growth constants $A = 9 \cdot 10^{-11}$ m/cycle and $m = 2.2$, and a propagation threshold $\Delta K_{th} = 8.1$ MPa√m, all measured under $R = 0.05$. The size of the process zone is calculated from

Equations (7-10), resulting in $\alpha = 6.97$, $\beta = 1.35$, $\gamma = 0.15$, and $b_f = 11.6 \times 10\mu m \cong 116\mu m$. Using the same process described previously, the delay cycles n_D is estimated by:

$$n_D = \int_{b_0}^{b_f} \frac{db}{A(\Delta K_b - \Delta K_{th})^m} - \int_{b_0}^{b_f} \frac{db}{A(\Delta K_I - \Delta K_{th})^m} = 33,961 - 16,645 = 17316 \qquad (12)$$

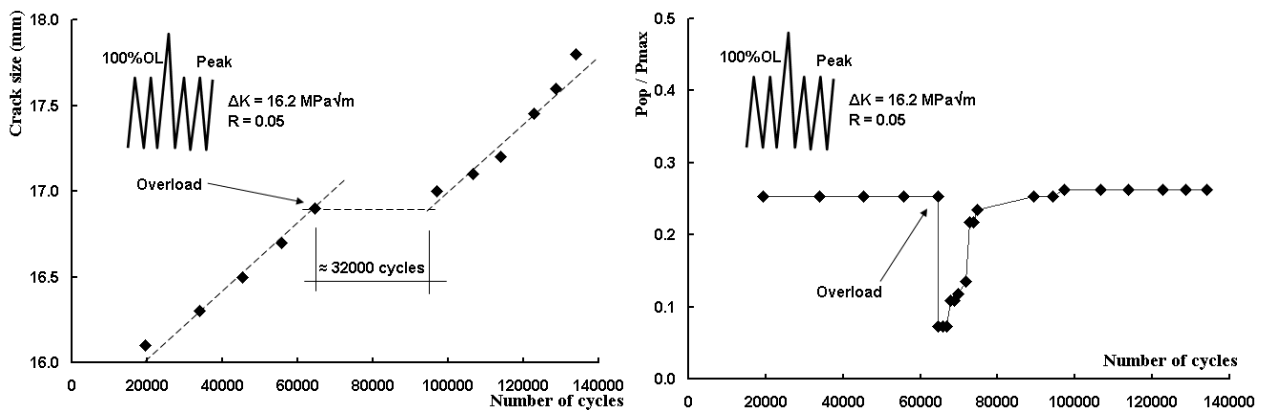which is about half of the measured 32,000 delay cycles, see Figure 7(a).

Figure 7. (a) Fatigue crack growth retardation after a 100 % overload, R = 0.05 (test II). (b) Opening load measurements, before and after the overload.

Note that in all tests there was no retardation induced by crack closure. The only test in which crack closure was detected was test II, however after the overload the opening load in fact decreased, see Figure 7(b). The opening load remained lower than before the overload along the entire process zone, only returning to its original value after the bifurcation effect had ended. Therefore, even if closure affected the constant amplitude growth behavior in test II, it would not be able to explain the measured overload-induced retardation. This behavior has already been verified in the literature (Meggiolaro and Castro, 2003).

The errors in the predictions performed using the proposed semi-empirical equations can be explained by inaccuracies in the estimation of the initial branch lengths b_0 and c_0, since the retardation effect is highly dependent on the ratio c_0/b_0. In addition, other retardation mechanisms besides bifurcation (except for closure, as discussed above) might be contributing to increase the number of delay cycles, such as unmodeled environmental effects or further kinking of the branch tips due to microstructure inhomogeneities. Another factor could be a specimen thickness effect, where the plane strain condition assumed in the 2-D calculations would result in less retardation than the actual 3-D stress state. However, the retardation mechanism behind a possible thickness effect in the performed experiments could not be crack closure, as shown in Figure 7(b). In any case, the presented predictions are of the same order of magnitude of the experimental scatter. Therefore, the quantitative approach presented in this work is a quite promising tool for modeling and calculating overload-induced retardation effects where other mechanisms have failed to give a satisfactory explanation.

4. Conclusions

In this work, a specialized FE program was used to calculate the propagation path and associated stress intensity factors (SIF) of bifurcated cracks, which can cause crack retardation or even arrest. A total of 262 crack propagation simulations were obtained from 6,250 FE calculation steps to fit empirical equations to the process zone size and crack retardation factor along the curved crack branches. In particular, the bifurcation simulations included several combinations of bifurcation angles $2\theta = \{40^o, 80^o, 90^o, 130^o, 168^o\}$, branch asymmetry ratios $c_0/b_0 = \{0.5, 0.7, 0.8, 0.9, 0.95, 1.0\}$, crack growth exponents $m = \{2, 3, 4\}$, and even considered interaction between crack branching and other retardation mechanisms through the threshold ratios $K_{PR}/K_I = \{0.0, 0.067, 0.08, 0.10, 0.13, 0.20, 0.25, 0.40, 0.57\}$. It was shown that very small differences between the lengths of the bifurcated branches are sufficient to cause the shorter one to eventually arrest as the longer branch returns to the pre-overload conditions. The process zone size was found to be smaller for lower bifurcation angles and for branches with greater asymmetry, in both cases due to the increased shielding effects on the shorter branch. The retardation zone was reduced as well for materials with higher crack growth exponents, due to the increased difference between the crack growth rates of the longer and shorter branches. Higher K_{PR} levels also resulted in smaller process zones, because the shorter branch was more easily arrested due to the reduction in its stress intensity range. However, a competition between smaller process zone sizes and lower growth

rates of the longer branch did take place to determine the real effect of combined bifurcation and other retardation mechanisms. The proposed equations, besides capturing all above described phenomena, can be readily used to predict the propagation behavior of branched and kinked cracks in an arbitrary structure, as long as the process zone is small compared to the other characteristic dimensions. It should be recognized however that the presented mixed-mode equations are only accurate if the branch lengths greatly exceed the size scale of the microstructural inhomogeneities and the size of the near-tip plastic zone. But assuming that the entire crack-front bifurcates uniformly, as observed in this work from scanning electron micrographs, the specimen thickness itself may provide the size scale requirements for the validity of the presented equations, as the calculated SIF may be averaged considering the (several) grains present along the thickness. From these results, it can be seen that crack bifurcation may provide an alternate mechanistic explanation for overload-induced crack retardation on structural components, especially to explain load interaction effects under closure-free conditions.

5. References

ASTM Standard E 647. "Standard Test Method for Measurement of Fatigue Crack Growth Rates". ASTM Standards;03.01.

Castro, J.T.P., 1993, "A Circuit to Measure Crack Closure". Exp. Techniques, Vol.17, N.2, pp.23-25.

Erdogan, F., Sih, G.C., 1963, "On the Crack Extension in Plates under Plane Loading and Transverse Shear". Journal of Basic Engineering. Vol.85, pp.519-527.

Karihaloo, B.L., 1982, "On Crack Kinking and Curving". Mechanics of Materials, Vol.1, pp.189-201.

Lang, M., Marci, G., 1999, "The influence of single and multiple overloads on fatigue crack propagation". Fatigue and Fracture of Engineering Materials and Structures, Vol.22, pp.257-271.

Lankford J., Davidson D.L., 1981, "The Effect of Overloads upon Fatigue Crack Tip Opening Displacement and Crack Tip Opening/Closing Loads in Aluminum Alloys". Advances In Fracture Research, Perg.Press, Vol.2, pp.899-906.

Meggiolaro, M.A., Castro, J.T.P., 2003, "On the dominant role of crack closure on fatigue crack growth modeling". International Journal of Fatigue, Vol.25, N.9-11, pp.843-854.

Miranda, A.C.O., Meggiolaro, M.A., Castro, J.T.P., Martha, L.F., Bittencourt, T.N., 2002, "Fatigue Crack Propagation under Complex Loading in Arbitrary 2D Geometries". ASTM STP 1411, Vol.4, pp.120-146.

Miranda, A.C.O., Meggiolaro, M.A., Castro, J.T.P., Martha, L.F., Bittencourt, T.N., 2003, "Fatigue Life and Crack Path Prediction in Generic 2D Structural Components". Eng. Fracture Mechanics, Vol.70, pp.1259-1279.

Pärletun, L.G., 1979, "Determination of the growth of branched cracks by numerical methods". Engineering Fracture Mechanics, Vol.11, pp.343-358.

Sadananda, K., Vasudevan, A.K., Holtz, R.L., 2001, "Extension of the Unified Approach to Fatigue Crack Growth to Environmental Interactions". International Journal of Fatigue, Vol.23, pp.S277-S286.

Suresh, S., 1983, "Crack Deflection: Implications for the Growth of Long and Short Fatigue Cracks". Metallurgical Transactions, Vol.14a, pp.2375-2385.

Suresh, S., Shih, C.F., 1986, "Plastic Near-tip Fields for Branched Cracks". International Journal of Fracture, Vol.30, pp.237-259.

6. Responsibility notice

The authors are the only responsible for the printed material included in this paper.